BEHAVIOR OF SAND AFTER LIQUEFACTION

by
Nozomu YOSHIDA[1], Susumu YASUDA[2], Masanori KIKU[3],
Tamio MASUDA[4], and W.D. Liam FINN[5]

ABSTRACT

Behavior of sand after liquefaction is discussed and formulated. Material properties that are usually assumed constant, such as internal friction angle, is ahown to change due to cyclic loading causing liquefaction. It is also shown that regions with very small stiffness appears by the cyclic loading. They may expand several ten percents, which causes liquefaction-induced large permanent displacement. A simlified model is introduced and improved so as to be able to take into new features such as change of material property and appearance of low stiffness region. The agreement of the numerical calculation and test are very good. Future research needs for evaluating the amount of liquefaction-induced permanent displacement more precisely are also pointed out.

[1] Engineering Research Institute, Sato Kogyo Co., Ltd., Atsugi, Japan

[2] Department of Civil Engineering, Tokyo Denki University, Saitama, Japan

[3] Department of Civil Engineering, Yokohama National University, Yokohama, Japan

[4] Civil Engineering Hydro Generation and Transmission Engineering Department, Tokyo Electric Co., Ltd , Tokyo, Japan

[5] Department of Civil Engineering, University of British Columbia, Vancouver, Canada

INTRODUCTION

Since Hamada et al. (1986) found that large permanent displacement (lateral spreading) occurred when soil liquefied in a widespread area, many efforts have been done to find the mechanism of lateral spreading caused by liquefaction and to evaluate the amount of lateral spreading (Hamada et al., 1994). Through the studies such as shaking table test (Yasuda et al., 1992, for example) and investigation of piles damaged due to lateral spreading (Yoshida et al., 1992; Yoshida and Hamada, 1992), it have been clarified that large deformation occurs in whole liquefied layer but not in a particular slip plane.

Figure 1 shows the mechanism of lateral spreading based on these observations schematically. Line ℓ denotes a backbone curve at the beginning of the earthquake. At this stage, nonzero shear stress exists in the horizontal plane mainly because of the gravity load when the ground is not a level ground. Point A in Figure 1 is then supposed to be an initial state.

When excess pore water pressure generates, material properties such as shear strength and elastic moduli change. Suppose that the backbone curve moves from ℓ to m by the change of material property. Because driving shear stress is caused by gravity, it hardely change under the small change of material property. If it does not change, the state point moves from A to B. Therefore, shear strain increases by the amount of γ_2-γ_1. As shown in this example, additional shear strain is generated if excess pore water pressure generates.

The amount of shear strain increases according to the generation of the excess pore water pressure. If the driving stress keeps constant, shear strain becomes infinite when shear strength becomes less than the driving stress. However, in the actual ground, the driving stress also decreases according to the change of geometry. Therefore actual strain increment from state ℓ to state m is not from A to B but from A to C. In other word, strain increment caused by the change of material property is not γ_2-γ_1 but γ_3-γ_1. Lateral spreading stops when new material property comes to a balance with a new driving stress, which is shown as point D in the figure.

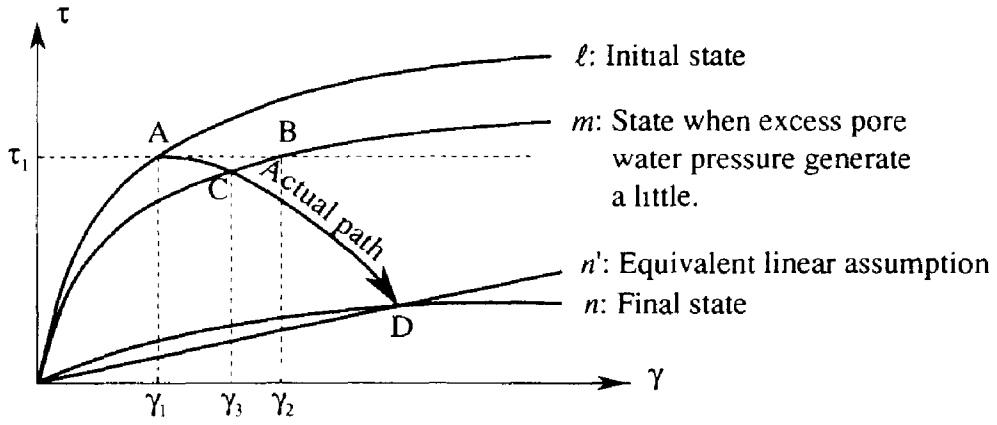

Figure 1 Schematic figure showing the mechanism of lateral spreading

This illustration implies two important features for predicting the amount of lateral spreading. The one is a stress-strain relationship to large strains and the other is a consideration of the change of geometry or large deformation theory.

Several analytical methods have been proposed for predicting the magnitude of lateral spreading based on this mechanism. Yoshida (1989) and Finn et al. (1991) used hyperbolic stress-strain relationships and large deformation theory. However, these methods require lots of computing time because both the change of geometry and that of material property must be considered in the same time. A more simplified methods have also been proposed. Employment of linear stress-strain relationship or zero stiffness on the liquefied layer is one simplification. Towhata et al. (1992) assumed zero stiffness and derived an analytical solution. Yoshida (1990) used equivalent linear concept in the FEM analysis. Yasuda et al. (1992) uses additional simplification, small deformation theory, in addition to linear stress-strain relationship.

In these analyses, stiffness of liquefied layer is assumed to be zero or very small except Finn et al. (1991) who dealt with partial liquefaction as well as complete liquefaction. By this zero stiffness assumption, we may be able to predict maximum possible displacement. In other word, it may be valid if we want to compute the displacement when a tilted ground becomes horizontal. However, all the liquefied ground does not always become a level ground. It is also obvious that the stiffness and the residual strength after the liquefaction affect the displacement prediction very much. In this paper, we discuss the behavior of sand at large strains and that after the liquefaction from the point of view for developing the stress-strain model based on test result.

BRIEF DESCRIPTION OF LABORATORY TEST AFTER LIQUEFACTION

Toyoura sand, with relative density from 30% to 70%, is tested by means of torsional shear test apparatus (Yasuda et al., 1993). Figure 2 shows loading program schematically. Specimen is formed and isotropically consolidated to an effective mean stress p'=0.5kgf/cm^2. Then shear stress with constant amplitude is applied until the safety factor against liquefaction, F_L, decreases to a specified value. Finally, load is applied so that shear strain increases monotonically. The second stage (cyclic loading) and the third state (monotonic loading) of test are conducted under an undrained condition. Only the behavior at the 3rd loading stage is shown and discussed hereafter.

Figure 3(a) shows examples of test result. Here, "static" indicates the test in which there is no cyclic load (2nd stage loading in Fig.2) before monotonic loading. Big difference is seen between the results of static and the of other loadings (called "post-liquefaction loading" hereafter). Shear stress at the beginning of the monotonic loading is nearly zero in the post-liquefaction loading. Figure 3(b) focuses on the behavior at small stresses. The stiffness at the beginning of loading is very small, but not zero although loading starts after the soil liquefied. At certain strain, the sand recovers its stiffness very rapidly, and, as seen in Fig. 3(a), stiffness finally becomes comparable order with the one of static loading. The former part is called low stiffness region and the latter high stiffness region hereafter. Our goal is to predict the behavior of sand in whole these region.

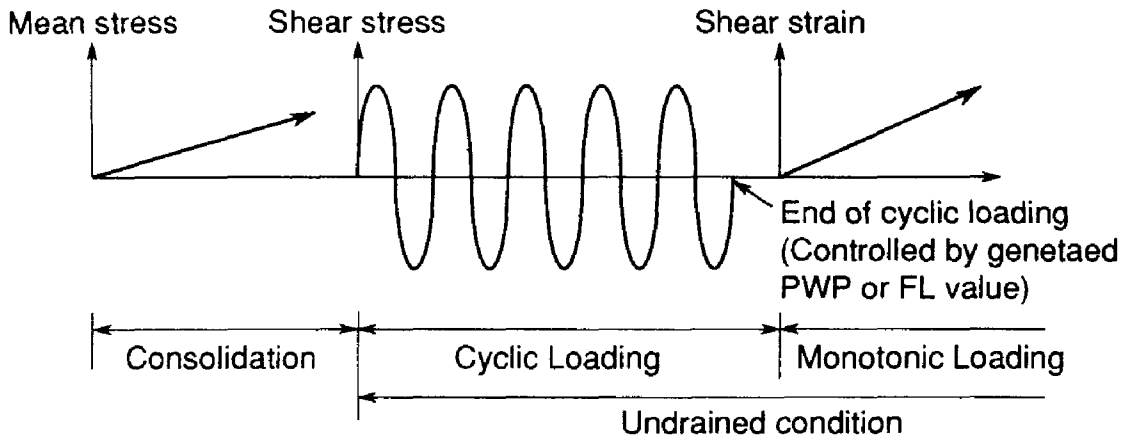

Figure 2 Loading program

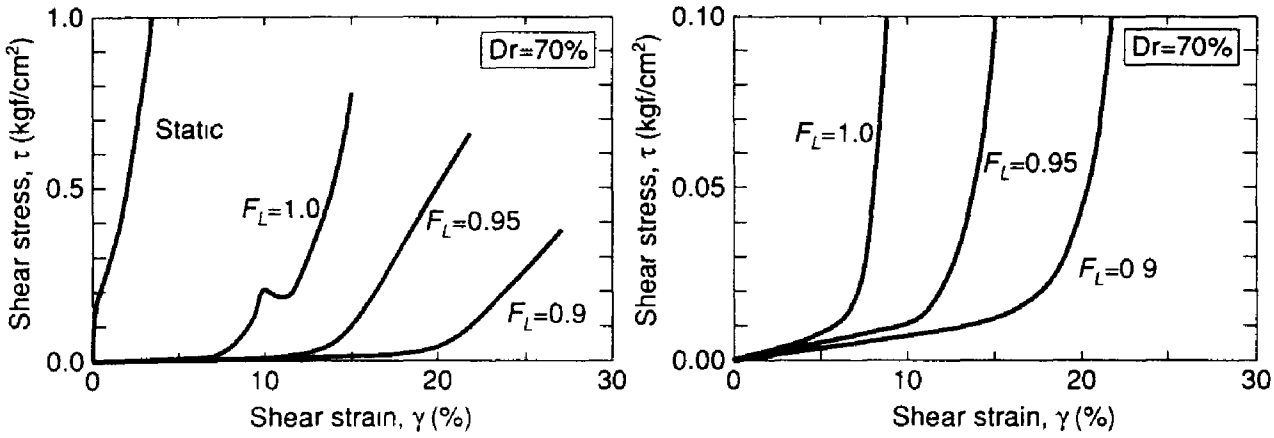

(a) Whole test result (b) Behavior at small stress

Figure 3 Stress-strain relationship of typical test results

BASIC EQUATIONS OF STRESS-STRAIN MODEL

A simplified method (Yoshida et al., 1993a,b) is employed for formulating the basic stress-strain model. Although this method includes wide scope including cyclic plasticity, the simplest form is used so as to make the characteristics of the behavior of sand clear.

Deformation of soil is divided into volume change and shear deformation. Incrementally elastic behavior is assumed for the volume change;

$$dp' = K\left(d\varepsilon_v - d\varepsilon_{vd}\right) \tag{1}$$

where

p' : effective mean stress

$K = K_o p'^n$: tangent bulk modulus (2)

K_o : bulk modulus constant

n : bulk modulus exponent

ε_v : volumetric strain

ε_{vd} : volume change due to dilatancy

Volume change ε_{vd} due to dilatancy is computed by using the generalized stress-dilatancy relationship,

$$\frac{d\varepsilon_{vd}}{d\gamma} = \mu - \frac{\tau}{p'} \tag{3}$$

where γ denotes equivalent shear strain, and τ denotes equivalent shear stress (radius of Mohr's cycle). The variable μ is a parameter, but, at present, we put $\mu=\mu_p$ following the ordinary stress-dilatancy relationship, where and μ_p denotes stress ratio τ/p' at phase transform. From Eqs. 1 and 3, we can compute effective mean stress increment for given strain increment $d\varepsilon_{ij}$. Therefore, the value of effective mean stress is known when computing shear deformation in the followings.

Hyperbolic model is employed for shear stress-shear strain relationship, which is expressed in the dimensionless form as

$$\eta = \frac{\xi}{1+\xi} \tag{4}$$

where

$\eta = \tau / \tau_{max}$: shear stress ratio

$\tau_{max} = p' \sin\phi$: shear strength (5)

ϕ : internal friction angle

$\xi = \frac{\gamma G_{max}}{\tau_{max}}$: shear strain ratio

G_{max} : shear modulus at small strains

Since effective mean stress is already known, both G_{max} and τ_{max} are known quantities. Dimensionless tangent shear modulus g is obtained by differentiating η with respect to ξ, which yields

$$g = \frac{d\eta}{d\xi} = \frac{1}{(1+\xi)^2} \tag{6}$$

Finally, deviatoric stress increment ds_{ij} is obtained from the given deviatoric strain increment $d\gamma_{ij}$ as

$$ds_{ij} = g\, G_{max} d\gamma_{ij} \tag{7}$$

Stress increment is computed from Eqs. 1 and 7.

This formulation is shown to be effective for simulating the behavior of sand in the ordinary shear strain range up to several percent (Yoshida et al., 1993b). However, it does not seem to be valid at very large strains or for the behavior after liquefaction, which will be discussed hereafter. The formulation will be improved based on the discussion of the characteristics of the behavior of sand both at large strains and after the liquefaction.

BEHAVIOR OF SAND AT LARGE STRAINS

In this section, we discuss the stress-strain relationship at large strains where stress point moves along the failure surface. Equivalent shear strain increment $d\gamma$ is easily computed from a given strain increment $d\varepsilon_{ij}$. Then, volumetric change due to dilatancy is computed from Eq 3. Under the undrained condition, however, this volume change does not occur, but effective mean stress changes

by the amount of

$$dp' = -K d\varepsilon_{vd} \tag{8}$$

Substitution of Eq.3 into Eq.8 yields

$$dp' = K\left(\frac{\tau}{p'} - \mu\right)d\gamma \tag{9}$$

Since the stress path moves along the failure surface, the stress ratio τ/p' is approximately expressed as

$$\frac{\tau}{p'} = \sin\phi \tag{10}$$

Therefore, Eq.9 yields

$$dp' = K(\sin\phi - \mu)d\gamma \tag{11}$$

Shear strength increment $d\tau_{max}$ during the change of mean effective stress is computed from Eq. 5 as

$$d\tau_{max} = dp' \sin\phi \tag{12}$$

We again use the assumption that stress path moves along the failure surface. Then, equivalent shear stress increment $d\tau$ is nearly equals to the shear strength increment $d\tau_{max}$. Finally, we obtain stress-strain relationships at large strains in the incremental form

$$d\tau = K(\sin\phi - \mu)\sin\phi \cdot d\gamma \tag{13}$$

Equation 13 implies that a computed stiffness at large strains is strongly affected by the value of μ, because other parameters are well known physical quantities.

The value of μ for static loading is back calculated from Eq. 13 and $d\tau/dp'$ value read off from the test result. Here tangent bulk modulus is computed from

$$K = \frac{2(1+\nu)}{3(1-2\nu)}G_{max} \tag{14}$$

where ν denotes Poisson's ratio. Shear modulus G_{max} at small strains is computed from the empirical equation for Toyoura sand (Kokusho, 1980),

$$G_{max} = 840\frac{(2.17-e)^2}{1+e}p'^{1/2} \quad (\text{kgf/cm}^2) \tag{15}$$

where e denotes void ratio. Kokusho (1980) also showed Poisson's ratio ν as a function of effective confining pressure as shown in Fig. 4. The value at p'=0.5kgf/cm^2 is used in Eq. 14 and the following analysis.

Figure 5 shows computed μ value at large strains, μ_f . The value of μ increases with relative density. This tendency is quite different with the tendency of phase transformation angle which decreases with relative density. Therefore it is obvious that we cannot obtain good prediction at large strains if $\mu=\mu_p$ is used at large strains.

The change of μ value from stress ratio $\eta=\mu_p$ (phase transform) to $\eta=1$ (on failure line) is not known. In the followings, therefore, we use piecewise linear relationship between μ and η. Figure 6 shows the result of analysis for static loading. The agreement between test and analysis is very good.

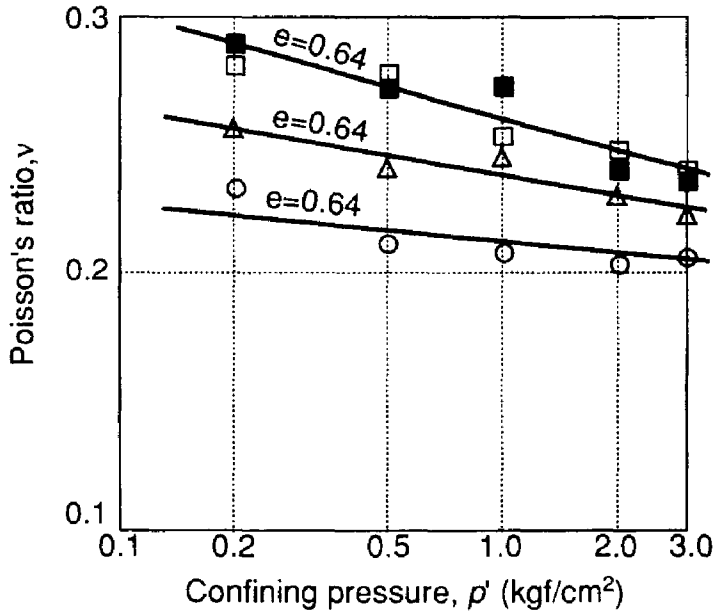

Figure 4 Poisson's ratio versus effective mean stress relationship (Kokusho, 1980)

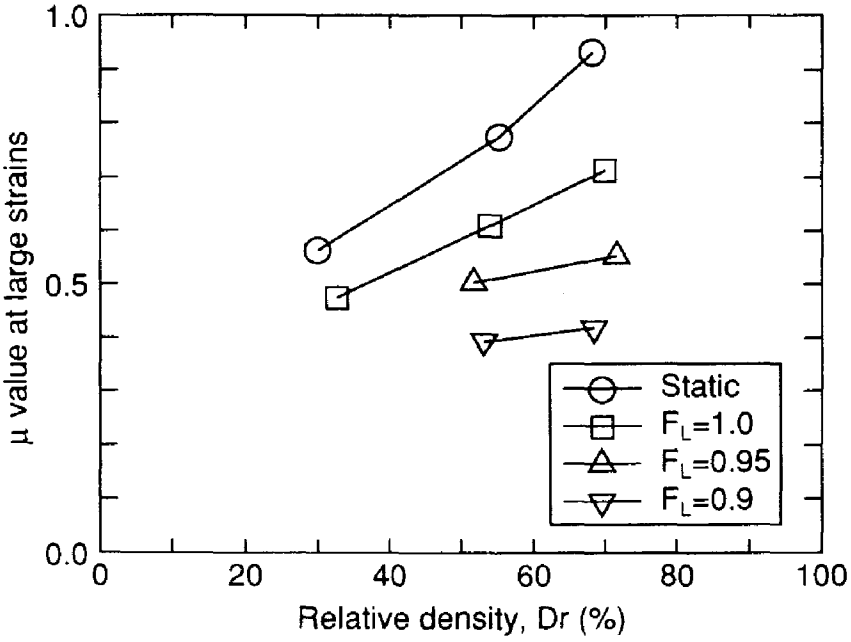

Fig.5 The value of μ at large strains

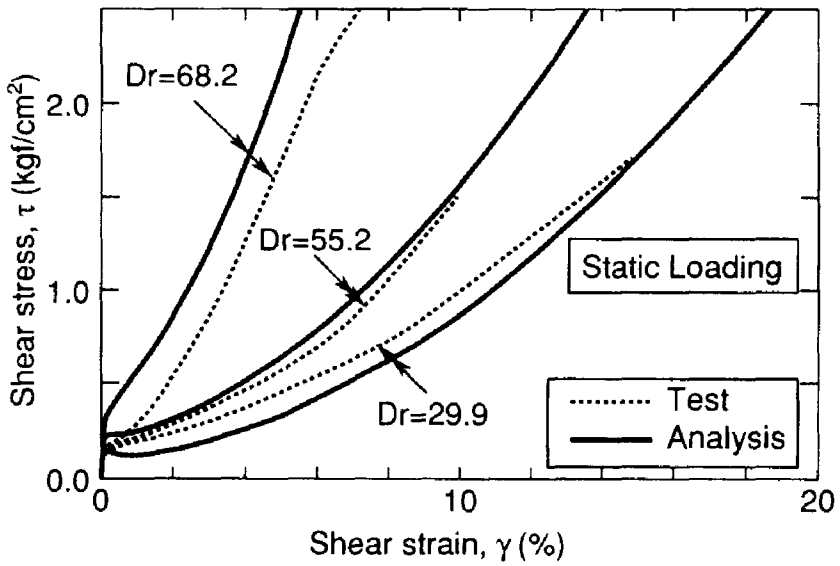

Fig.6 τ-γ relationship for static loading

EFFECT OF OCCURRENCE OF LIQUEFACTION

In almost all constitutive models, material properties with physical meanings such as internal friction angle are assumed to be constant even if liquefaction occurs. As the first trial, therefore, we use similar method; the effect of liquefaction is considered only in the initial condition. Because of the occurrence of liquefaction, effective mean stress decreases very much. So, we use 1/100 of initial effective mean stress, p_o=0.005kgf/cm^2, as initial mean stress.

Figure 7 shows the result of analysis in comparison with test and previous analysis. This analysis (p_o=0.005kgf/cm^2) generates more strain than previous analysis (p_o=0.5kgf/cm^2), which comes from the difference between the behaviors at the beginning of the loading. This analysis starts at very low effective mean stress, therefore stiffness at the beginning is also small, which is the reason why this analysis generates more strain than the previous. However, as discussed in the previous section, this analysis does not improve the behavior at large strains; stress-strain curves are almost parallel to each other. In addition, stiffness at the beginning of loading in this analysis is much smaller than the one by previous analysis, but it is still much larger compared with test results of post-liquefaction loading. Therefore, the resultant strain is still much smaller than the ones of tests with post-liquefaction loading.

Observation of both test result and detailed comparison between test and analysis show following disagreements.

1) Analysis shows larger stiffness at the beginning of loading, because low stiffness region observed in the test is not considered in the analysis.
2) Stiffness at high stiffness region by test decreases depending of F_L, but constant in the analysis.
3) The behavior of post-liquefaction loading changes depending on F_L value, but it is not considered

in the analysis.

These facts imply that material property may change during the cyclic loading conducted before the post-liquefaction loading. In the following sections, we will discuss these and consider the effect of liquefaction in developing the stress-strain modeling.

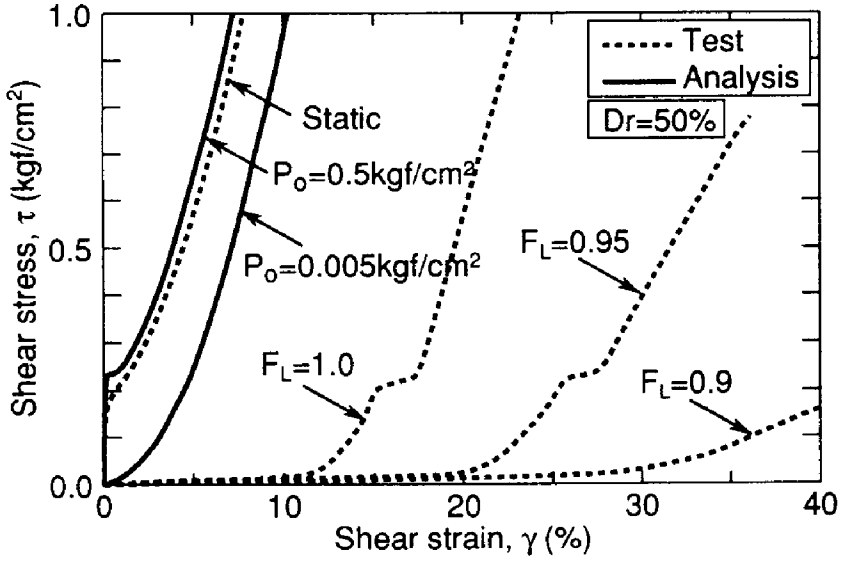

Figure 7 Comparison of stress-strain relationship

INTERNAL FRICTION ANGLE AND PHASE TRANSFORM

Figure 8 shows an example of stress paths of the test of relative density 70%. The stress-strain relationship of this test is shown in Fig. 3. Stress path moves linearly after phase transformed for static loading test. It moves almost linearly from the beginning of loading for post-liquefaction loading test. Therefore, stress point is supposed to move along the failure line. It is clearly observed that the slope decreases with F_L value, which implies that internal friction angle changes depending on the loading before the monotonic loading.

The slope angles are read from stress path trajectory and plotted in Fig. 9. Those obtained from tests with other relative deisities are also plotted in the figure. Here, it is noted that this angle is not an internal friction angle ϕ, but $\tan^{-1}(\sin\phi)$. The dependency of internal friction angle on the loading before liquefaction is also clearly observed.

Phase transform is very difficult or impossible to read from test result of post-liquefaction loading. According to the parametric studies using the final form of the stress-strain model of this paper, however, μ_p value does not affect the whole behavior very much. Therefore, in the following analysis, it is held constant regardless of F_L value.

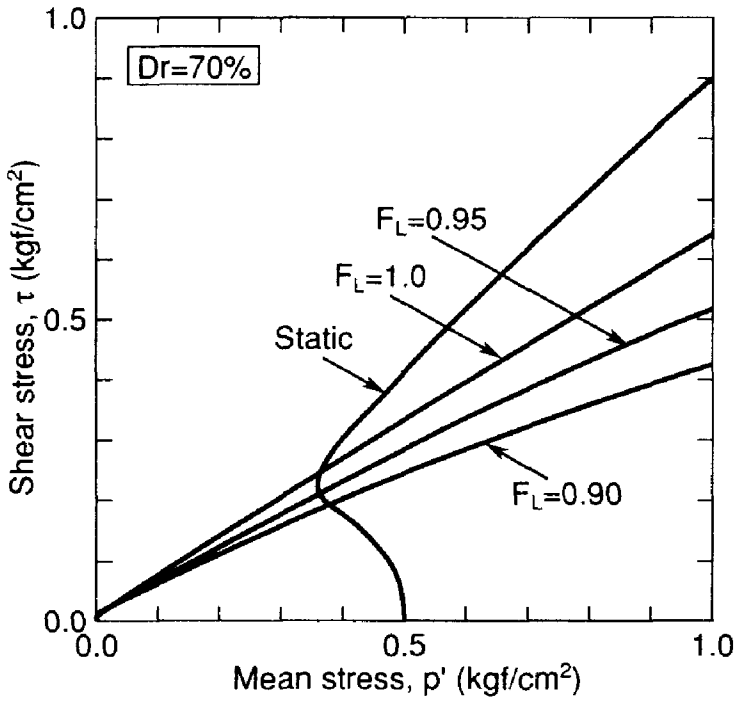

Fig.8 Stress path of test with relative density of 70%

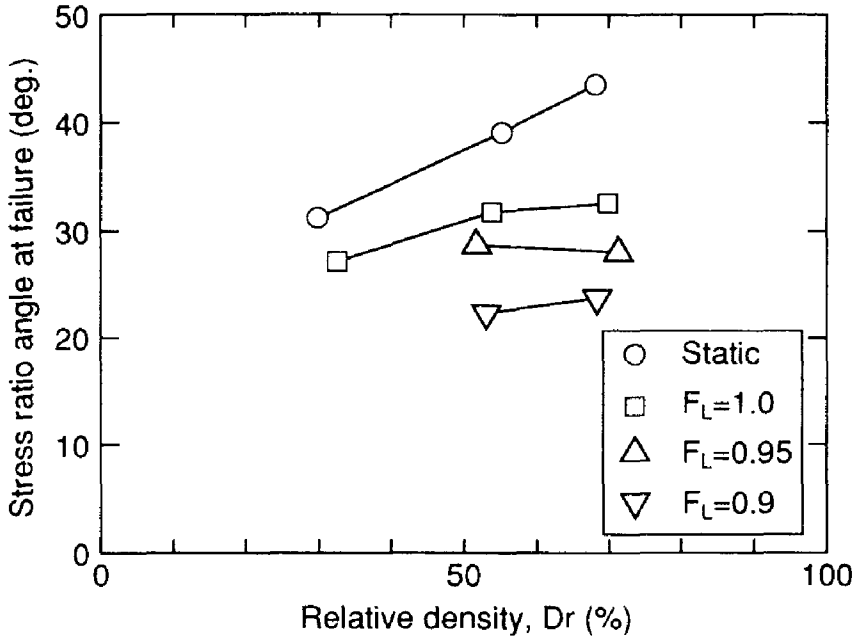

Fig. 9 Change of slope of failure line caused by liquefaction

Knowing the internal friction angle and the slope of the stress-strain curve at high stiffness region, the value of μ_f can be calculated. The result is overplotted in Fig. 5. The value of μ_f decreases as F_L value decreases or cyclic loading after liquefaction increases, which is the similar to the tendency of internal friction angle.

EVALUATION OF LOW STIFFNESS REGION

It is easily recognized from the previous analysis that modification of internal friction angle and μ value will improve the behavior in high stiffness region, but not in low stiffness region. Yoshida et al. (1994) measured the relationship between the volumetric strain and effective mean stress during the process of excess pore water pressure dissipation so as to obtain the settlement characteristics of the ground after liquefaction by means of triaxial shear test apparatus. Figure 10 shows typical result of the test.

The p'-ε_v relationship is divided into two parts. At the beginning of drainage, bulk modulus is very small. It increases very rapidly at certain volumetric strain. This behavior is similar to the test result described in the previous section; low stiffness region and high stiffness region correspond to low and high bulk modulus regions, respectively. The p'-ε_v relationship shown in Fig. 10 is obtained on the process of excess pore water pressure dissipation. If principle of effective stress holds, however, the same relationship is valid for the undrained behavior discussed here.

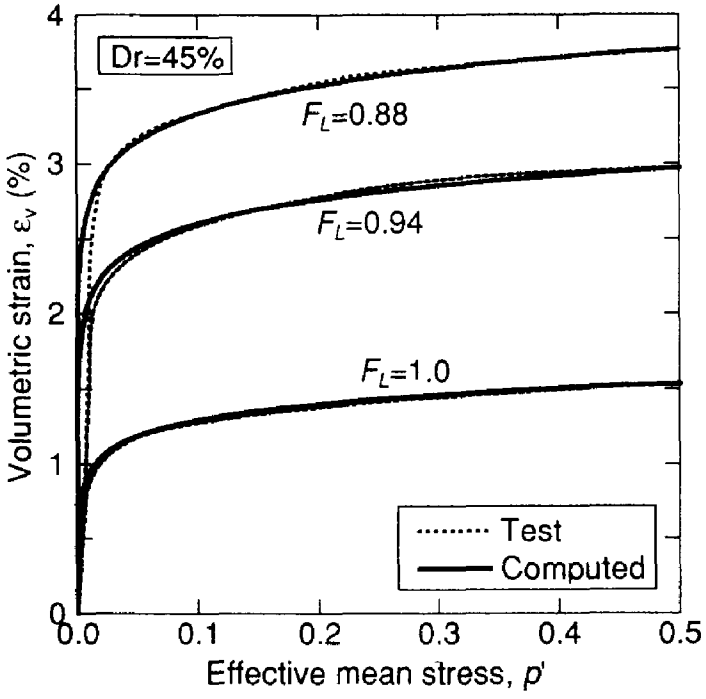

Fig.10 Volumetric strain characteristics during the excess pore water pressure dissipation after liquefaction. (Yoshida and Finn, 1994)

Since there is few change of shear strain on the process of drainage, volume change due to dilatancy is supposed not to include in the measured volumetric change in Fig.10. Yoshida et al. (1994) pointed out that bulk modulus at high bulk modulus region is consistent to the bulk modulus derived from ordinary empirical equation such as Eq. 2. This implies that elastic modulus (tangent bulk modulus) is very small in the low bulk modulus region. If so, it is also reasonable to assume that shear modulus G_{max} at small strains is also very small. Otherwise, Poisson's ratio becomes very small or negative. which is not realistic.

Yoshida and Finn (1994) formulates the behavior in Fig. 10 in the following equation,

$$\frac{p'}{p'_o} = \frac{e^{\frac{\varepsilon_v}{c}} - 1}{e^{\frac{\varepsilon_{vo}}{c}} - 1} \tag{16}$$

where p'_o denotes initial effective mean stress from which cyclic load is applied to cause liquefaction, and ε_{vo} denotes a volumetric strain at $p' = p'_o$. The variable c is a parameter, which is expressed as

$$c = 0.053\varepsilon_{vo} + 7 \times 10^{-4} \tag{17}$$

Tangent bulk modulus to be used instead of Eq. 2 is obtained from Eq. 16 as a function of effective mean stress p' as

$$K = \frac{1}{c} \frac{p'_o + p'(e^{\frac{\varepsilon_{vo}}{c}} - 1)}{e^{\frac{\varepsilon_{vo}}{c}} - 1} \tag{18}$$

The shear modulus G_{max} at small strains is then obtained from Eq. 14, where, in the following analysis, the value of Poisson's ratio is kept constant.

In the following analysis, tangent bulk modulus and shear modulus at small strains derived from Eqs. 18 and 14 are used, which covers both low and high stiffness regions. Here, it is noted that ε_{vo} in Eq. 16 was actual value which occurs after excess pore water pressure dissipates, but, when using in the analysis here, it is a fictitious value.

RESULT OF ANALYSIS AND DISCUSSION

In the first part of this paper, we introduced a basic form of stress-strain model, and after that, we have discussed the effect of liquefaction on the behavior of sand at large strains. From the point of view for computing the behavior of soil, they are summarized as follows;

1) Internal friction angle changes during the cyclic loading causing liquefaction, which is shown in Fig.9.
2) The value of μ at phase transform and that at large strains where stress path moves along the failure line are different to each other; the latter is generally larger than the former. Piecewise linear relationship is used in terms of shear stress ratio in this analysis. The value of μ_f is shown in Fig.5, which also changes depending on the amount of cyclic loading.
3) Tangent bulk modulus K is computed from Eq. 18 instead of Eq. 2. Shear modulus G_{max} at small strains is computed from Eq. 14, where Poisson's ratio is kept constant.

In applying Eq. 18. the value of ε_{vo} is not known, because it can be obtained after excess pore water

pressure dissipates. Moreover, since only the test result with relative density of 45% is shown in Fig. 10, ε_{vo} at other relative densities cannot be obtained from the figure. Therefore, at first, we treat ε_{vo} as a fitting parameter.

Figures 11 to 13 show the result of analysis and test result. Here, the value of μ_f cannot be read from the test result of Dr=30% and F_L=0.95 and 0.9, therefore suitable value is assumed. The agreement of analysis with test result is very good for both low stiffness region and high stiffness region, although a little disagreement is seen at the transition between two regions.

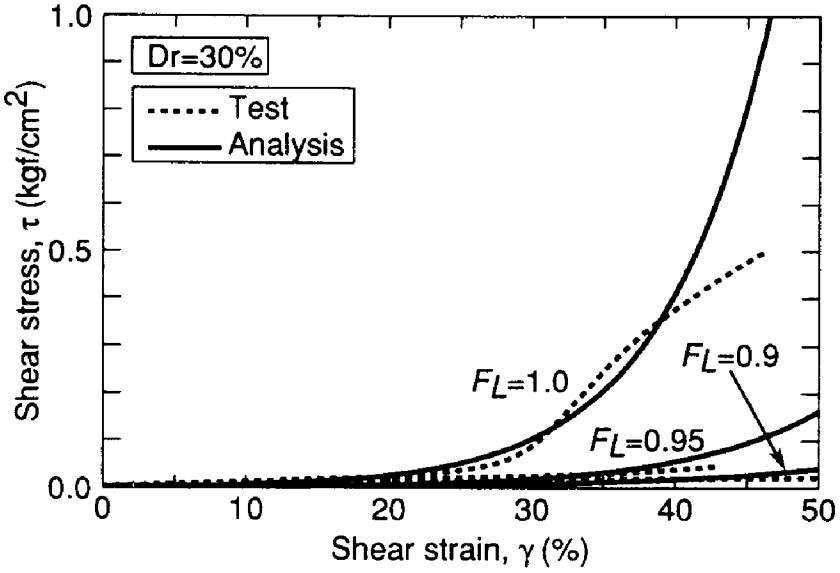

Fig.11 Stress-strain relationship for Dr=30%

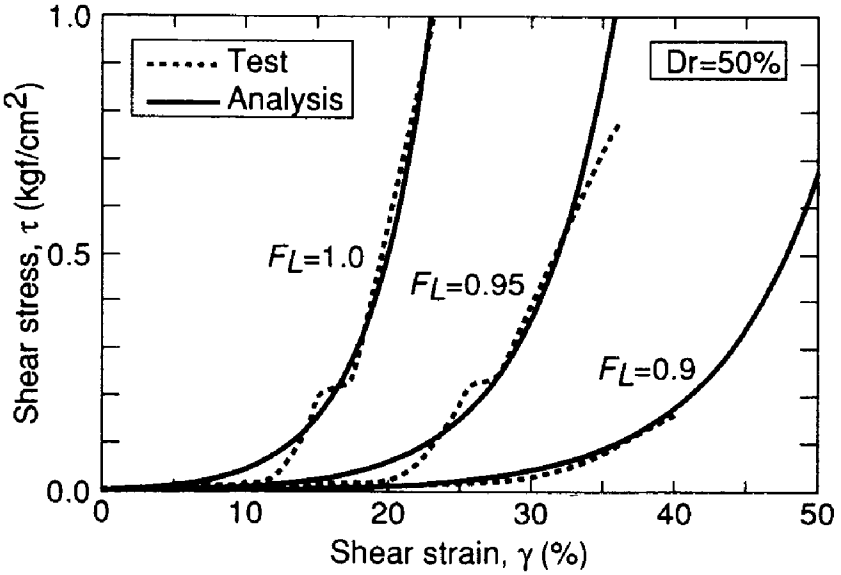

Fig.12 Stress-strain relationship for Dr=50%

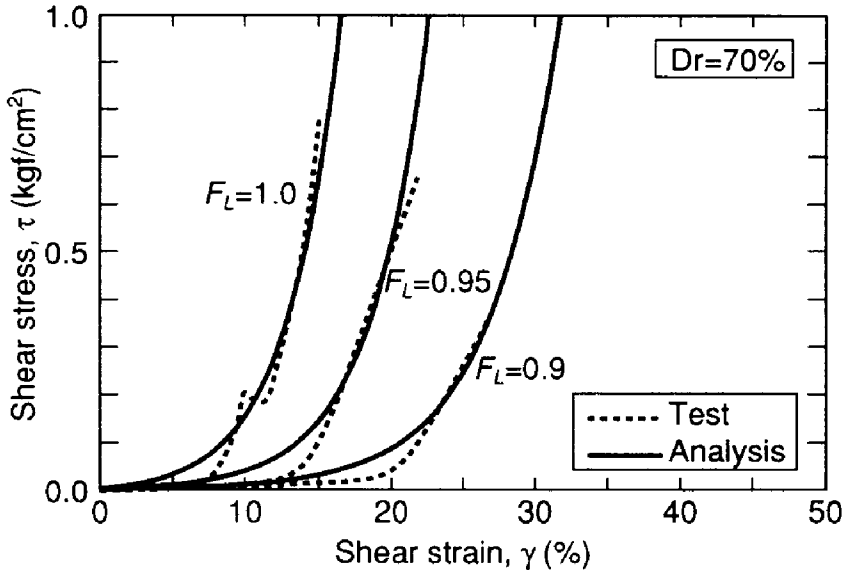

Fig.13 Stress-strain relationship for Dr=70%

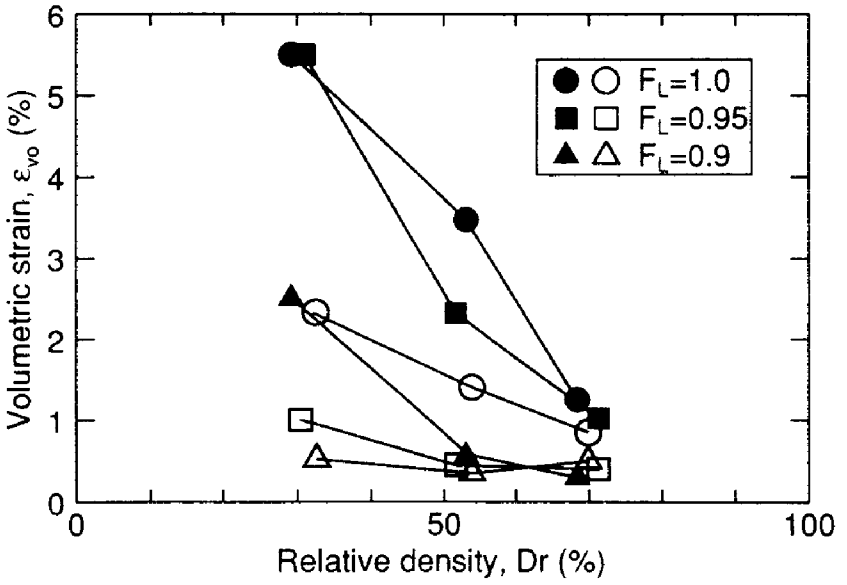

Fig. 14 Fictitious volumetric strain ε_{vo} used in the analysis

In Fig. 14, hollow symbols show evaluated ε_{vo} value in order to get good agreement as shown in Figs. 11-13. Ishihara (1993) produced a design charts as shown in Fig. 15 for evaluating the post-liquefaction volume change. This chart is derived based on random shear stress history loading by means of torsional shear test apparatus. The value of ε_{vo} can be read off from this figure from either F_L value or γ_{max} which is a maximum shear strain generated during the random loading. Here, it is noted that definition of the occurrence of liquefaction is different in the test described here and

Fig. 15. As seen in Fig. 15, F_L=1 corresponds to the generation of 3.5% shear strain under random loading. On the other hand, F_L=1 in the test discussed in this paper corresponds to the generation of 15% double amplitude shear strain under constant amplitude shear stress loading. Therefore, direct use of ε_{vo} value in Fig. 15 may not fit in the analysis. However, there is no direct conversion method. So, we try to use ε_{vo} value assuming that F_L values in both method are identical to each other in the next trial.

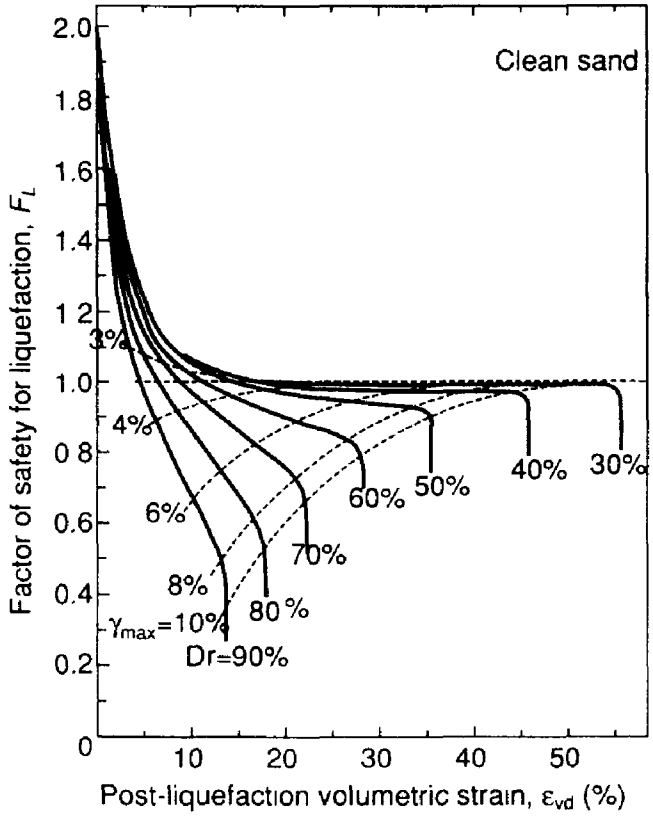

Fig.15 Design chart for obtaining post-liquefaction volumetric change (Ishihara, 1993)

Figure also 14 shows ε_{vo} value read off from Fig. 15 as solid symbols. it symbols is larger than that shown by hollow symbols. The value of ε_{vo} in the case of Dr=30% are the same for F_L=0.95 and 0.9. On the other hand, test result shown in Fig. 11 clearly shows more deterioration for F_L=0.9 than F_L=0.95 This also implies that F_L values in both test may not be of the same definition.

Since ε_{vo} shown by solid symbols in Fig. 14 (read off from Fig.15) is larger than that shown by hollow symbols (derived in this paper), it is obvious that new calculation gives larger low stiffness region than previous if other parameters are kept constant. As shown previously, all the parameters except μ have clear physical meanings in the theory proposed here. Therefore, we treat μ as fitting parameter and get better agreement with test result. Figure 16 shows the result of analysis for Dr=70%. The agreement with test result is also good although the agreement of the stiffness at high stiffness region is a little worse than previous.

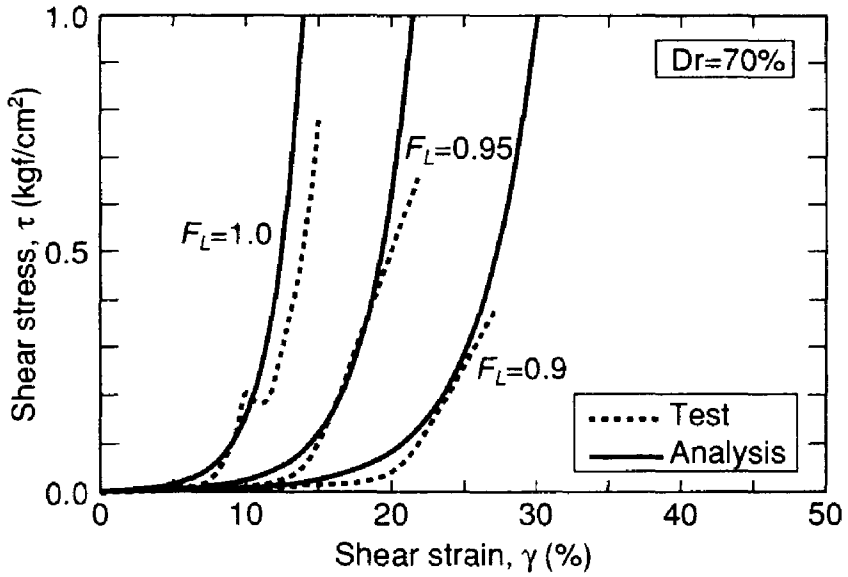

Fig. 16 Comparison between test and analysis in which fictitious volumetric strain shown in Fig. 15 is used and μ is treated as fitting parameters

CONCLUDING REMARKS

Several new features are presented in this paper from the point of view to predict the behavior of sand after liquefaction. The biggest one is the appearance of low stiffness region whose size depends on the amount of cyclic loading. The stiffness of this region is very small, and the strain is as large as several ten percents, which is a sufficient order of shear strain to cause large amount of liquefaction-induced permanent deformation. It may be recognized that this region occurs because soil particle configuration is very unstable, possibly floating up in the pore water or just close to that. The phase change from low stiffness region to high stiffness region occurs because the soil particle comes to a new stable configuration. This concept explains the change of material property due to cyclic loading. Therefore, the mechanism of liquefaction-induced lateral spreading is quite different with the ordinary discussion on residual strength or steady state under monotonic loading without cyclic loading before it.

Several ten percents of shear strain may not be enough to explain the lateral spreading observed in, for example, Niigata city during the 1964 Niigata earthquake (Hamada et al., 1993) where more than 100% of shear strain is supposed to occur. The discussion in this paper is based on the behavior under undrained condition. If configuration of soil particle is unstable at low stiffness region, the configuration may be disturbed by seepage flow. This will create additional displacement. Additional displacement is larger as thickness of liquefied layer increases because seepage flow caused by the excess pore water pressure dissipation continue for long period.

It is also noted that low stiffness region is observed even at F_L=1.0. It implies that this stage appears even before the occurrence of liquefaction. However, constitutive models usually does not consider the appearance of this region.

We also showed that the behavior of soil can be computed with reasonable accuracy by considering the low stiffness region. However, some of the parameters were not evaluated well because empirical experience is short or not conducted to evaluate these values within required accuracy. Therefore, we employed relevant value by our judgement in this paper, which may not be best choice and result in disagreement. For example, Poisson's ratio is assume to be constant in this analysis, but, as shown in Fig.4, it depends on confining pressure. However, since it is not expressed in a formula and value at very low confining pressure is not shown, we do not consider p' dependency of Poisson's ratio. The same things occured for phase transform angle. Moreover, we used Eq. 16 but the validity of this equation is proved only in particular cases. The change of internal friction angle and μ by cyclic loading are also not formulated. Research is required to obtain these behavior and to develop the empirical formulae used in the analysis.

We used F_L value to express the loading causing liquefaction and after liquefaction, and ε_{vo} value as the index of low stiffness region. Obviously, these are not convenient parameters when developing the stress-strain models. Trials to find another, more convenient parameter are also required.

REFERENCES

Finn,W.D.L., Yogendrakumar,M., Ledbetter,R.H. and Yoshida,N. (1991), Analysis of liquefaction induced displacements, 7ICCMAG, pp.913-921

Hamada,M., Yasuda,S., Isoyama,R. and Emoto,K. (1986): Study on Liquefaction Induced Permanent Ground Displacement, Association for the Development of Earthquake Prediction, Tokyo

Hamada,M, O'Rouke,T.D. and Yoshida,N. (1994): Liquefaction-induced Large Ground Displacement, Performance of Ground and Soil Structures during Earthquakes, 13th ICSMFE, New Delhi, JSSMFE, pp.93-108

Ishihara (1993): Rankine lecture

Kokusho,T. (1980): Cyclic Triaxial Test of Dynamic Soil Properties for Wide Strain Range, Soils and Foundations, Vol.29, No.2, pp.45-60

Towhata,I. et al. (1992): Prediction of Permanent Displacement of Liquefied Ground by Means of Minimum Energy Principle, Soils and Foundations, Vol.32, No.3, pp.97-116

Yasuda,S. et al. (1992), The mechanism and a simplified procedure for the analysis of permanent ground displacement due to liquefaction, Soils and Foundations, Vol.32, No.1, pp.149-160

Yasuda,S., Kiku,H., Yoshida,N., Masuda,T. and Itafuji,S. (1993): Torsional Shear Tests on Post Liquefaction Behavior of Sand, Preprint, Japan-US Seminor on Dynamic Behavior and Failure of Ground, Napa Valley, California

Yoshida,N. (1989): Large Deformation Analysis of Liquefaction-induced Ground Displacement by

Reduced Integral Method, Proc., 3rd Symposium on Computational Mechanics, Japan Union of scientists, pp.391-396 (in Japanese)

Yoshida,N., Kobayashi,K. and Nakamura,S. (1990): An Investigation of Pile Foundation of a Building Damaged at the 1964 Niigata Earthquake, Tsuchi-to-Kiso, JSSMFE, Vol.38, No.6, pp.39-44 (in Japanese)

Yoshida,N. and Hamada,M. (1990): Damage to Foundation Piles and Deformation Pattern of Ground due to Liquefaction-induced Permanent Ground Deformations, Proc., 3rd Japan-U.S. Workshop on Earthquake Resistant Design of Lifeline Facilities and Countermeasures for Soil Liquefaction, San Francisco, CA

Yoshida,N. (1990): LIQLARD: A Computer Code for Large Ground Displacement due to Soil Liquefaction, Association for the Development of Earthquake Prediction (in Japanese)

Yoshida,N. (1991): State of Arts of Liquefaction Analysis, Symposium on the Problems of Earthquake Motion and Ground in Water-front Area, AIJ, pp.37-44 (in Japanese)

Yoshida,N. and Tsujino,S. (1993a): A simplified Practical Stress-strain Model for the Multi-dimensional Analysis under Repeated Loading, Proc., The 28th Japan National Conference of Soil Mechanics and Foundation Engineering, pp.1221-1224 (in Japanese)

Yoshida,N., Tsujino,S., Nakajima,T. and Yano,Y. (1993b): A Simplified Practical Model for the Use of Multi-Dimensional Analysis, Part 2, Consideration of Dilatancy, Proc., 48th Annual Conf. of the Japan Society of Civil Engineering, Vol.3, pp.1218-1219

Yoshida,N., Tsujino,S. and Inadomaru,K. (1994): Fundamental Study on the Resudual Settlement of Ground after Liquefaction, Proc.,49th Annual Conf. of the Japan Society of Civil Engineering, Vol.3, pp.

Yoshida,N. and Finn,W.D.L. (1994) . Joint Element for Liquefaction and Consolidation Analysis (in preparation)